Journal of Hazardous Materials 384 (2020) 121253

Contents lists available at ScienceDirect

Journal of Hazardous Materials

journal homepage: www.elsevier.com/locate/jhazmat

Fast degradation, large capacity, and high electron efficiency of chloramphenicol removal by different carbon-supported nanoscale zerovalent iron

Jiang Xu[a,b,*], Xue Liu[a], Zhen Cao[a], Weiliang Bai[b], Qingyang Shi[b], Yi Yang[a,*]

[a] State Key Laboratory of Estuarine and Coastal Research, East China Normal University, Shanghai, 200062, China
[b] Department of Civil and Environmental Engineering, Carnegie Mellon University, Pittsburgh, 15213, USA

GRAPHICAL ABSTRACT

ARTICLE INFO

Editor: Xiaohong Guan

Keywords:
Antibiotics
Emerging contaminants
Denitration
Dechlorination
Antibacterial activity elimination

ABSTRACT

It remains unclear that which kind of carbon support is better for improving the reactivity of nanoscale zerovalent iron (nZVI) without the adsorption effects of carbon. Finding appropriate contaminants that could be degraded by nZVI with high capacity and electron utilization is crucial for exploring the applications of nZVI. High degradation rate (up to 3.70 min^{-1}) and high capacity (up to 3000 mg g^{-1}) of antibiotic chloramphenicol ($C_{11}H_{12}Cl_2N_2O_5$, CAP) removal with high electron utilization (> 97%) was achieved by different carbon supported nZVI in this study. Carbon powder (CP) was found to be the best support, possessing good distribution and reactivity of nZVI. 99% of CAP was removed by CP-nZVI after 3 min, without the electron consumption via the side reaction between nZVI and water, suggesting that CAP could outcompete with water for the electrons from nZVI. The entire pathway of CAP removal was elucidated based on UPLC-MS/MS analysis. Partial degradation of CAP (denitration and dechlorination) was enough to take away the antimicrobial properties. These results suggest a promising application scenario of carbon supported nZVI for the remediation of CAP-contaminated water to reduce the antibiotic selection pressure of the environment.

---

[*] Corresponding authors at: State Key Laboratory of Estuarine and Coastal Research, East China Normal University, Shanghai, 200062, China.
E-mail addresses: jiangx2@andrew.cmu.edu (J. Xu), yyang@geo.ecnu.edu.cn (Y. Yang).

https://doi.org/10.1016/j.jhazmat.2019.121253
Received 5 June 2019; Received in revised form 1 September 2019; Accepted 17 September 2019

1. Introduction

Nanoscale zerovalent iron (nZVI) has been considered as a strong reductant with large specific surface area and high reactivity, and has gained many attentions due to its great potential for environmental remediation (Wang and Zhang, 1997; Joo et al., 2004; Nurmi et al., 2005; Xu et al., 2019a). nZVI technology for contaminants removal has been widely studied over the past two decades, and most of the studies focused on developing various nZVI-based materials to overcome the limitations of nZVI and exploring the applications of nZVI for various contaminants of concern (Tang et al., 2016).

One interesting research hotspot is to address the deficiencies of nZVI, such as easy aggregation, easy passivation, low utilization ratio, short reactive longevity, and so on (Phenrat et al., 2007; Hwang et al., 2014). Supporting nZVI on a matrix becomes a feasible and attractive option to inhibit the aggregation of nZVI. Based on the method simplicity and chemical homogeneity of nZVI, various matrices have been used to support nZVI particles to mitigate the aggregation, such as carbon materials (Hoch et al., 2008; Xu et al., 2012a), clay (Li et al., 2015), magnetite (Xu et al., 2013a, b), silica (Tang et al., 2015), layered double hydroxide (Sheng et al., 2016), zeolite (Arancibia-Miranda et al., 2016), and so on. Carbon is the most abundant element in the biosphere among these materials, and conforms best to the sustainable materials development (Titirici et al., 2015). Carbon materials with large surface area and unique structure have been considered as promising materials to support nZVI particles, and activated carbon, biochar, carbon nanotubes, and graphene are commonly used (Zou et al., 2016). Nevertheless, most studies on the carbon-supported nZVI included the adsorption by carbon and the reduction by nZVI of the probe contaminant (Wu et al., 2013; Chang et al., 2011; Xu et al., 2013c), the precise role of these carbon supports (e.g. the morphology of carbon supports and the resulted distribution of nZVI particles on these supports) in the reactivity of nZVI without adsorption has not been clearly compared and verified.

Another research hotspot of nZVI is studying the possible interactions between nZVI and uninvestigated/emerging contaminants besides extensively studied conventional heavy metals (Zou et al., 2016; Boparai et al., 2011), inorganic anions (Wu et al., 2013; Xu et al., 2012b), and chlorinated organics (Liu et al., 2005; Xu et al., 2016a). However, few studies investigate the toxicity of degradation products after the treatment by nZVI, such as the antibacterial activity after antibiotics degradation. Moreover, most studies focused on the reactivity of nZVI without considering the utilization of nZVI, that is how much electrons from nZVI are used to degrade the targeted contaminant (Liu et al., 2005). Generally, the electrons from Fe^0 would either reduce the contaminant or reduce the water to hydrogen, and the latter is considered as an undesirable reaction that would waste the electrons from Fe^0 and reduce its capacity (Qin et al., 2017; Li et al., 2018; Qiao et al., 2018). Hence, it is of great important to improve the selectivity of nZVI, such as sulfidation (Li et al., 2018; He et al., 2018; Lv et al., 2019; Xu et al., 2019b), or finding an appropriate contaminant that could be degraded by nZVI and outcompete water for the electrons. Hence, from the electron efficiency point of view, it is hypothesized that the faster the contaminant is reduced by nZVI, the higher the electron efficiency, which would further increase the capacity of nZVI for the contaminant reduction and lower the cost of nZVI.

As a special category of emerging organic contaminants, antibiotics in water have become an emerging threat to ecosystems and human health due to the generation of antibiotic-resistant bacteria and genes (Chen et al., 2017; Guo et al., 2018). However, the removal efficiencies of antibiotics by wastewater treatment plants are relatively low due to the lack of a special technology for this category of contaminants (Ahmed et al., 2017). A chlorinated nitroaromatic antibiotic chloramphenicol (CAP) was selected as the target contaminant to explore the application of nZVI for antibiotics degradation in this study. As an effective bacteriostatic pharmaceutical, CAP has still been used in many developing nations due to its low production costs and wide availability. The frequent detection and existence of CAP in surface water, underground water, and sewage influent and effluent in China have been widely reported (Hu et al., 2010; Zhao et al., 2017).

In this work, nZVI particles were supported onto different carbon materials, including activated carbon, biochar, nanoscale carbon powder, carbon nanotubes, and graphene oxide. The effect of the carbon support on the reactivity of nZVI was investigated without the effect of CAP adsorption by the carbon support. The degradation rate, capacity, electron efficiency, and antibacterial activity of CAP removal by supported nZVI were studied to assess the application potential of nZVI for CAP-contaminated water.

2. Experimental section

2.1. Chemicals

CAP was obtained from Aladdin Reagent (Shanghai) Co., Ltd. $NaBH_4$, $FeSO_4{\cdot}7H_2O$, NaOH, and HCl of analytical grade were purchased from the Sinopharm Group Chemical Reagent Co., Ltd. Activated carbon (AC) and graphene oxide (GO) were obtained from Jining Leadernano Tech. LLC. Nanoscale carbon powder (CP) and multi-walled carbon nanotubes (CNTs) were obtained from Beijing Dk Nano technology Co., Ltd. and Shenzhen Nanotech Port Co., Ltd., respectively. Bamboo wood derived biochar (BC) was prepared via heating the wood particles (0.6–2 mm) at 380 °C in a closed reactor inside the furnace under nitrogen gas at 2 atm. All the chemicals were used without further purification. Ultrapure water (pH = 7.0) was purged by nitrogen for 1 h prior to the use in nZVI preparation and batch experiments.

2.2. Preparations

nZVI and carbon-nZVI nanocomposites were prepared immediately before use. The entire experimental procedure was performed in a 1000 mL three-necked flask with nitrogen purging and stirring (500 rpm), located in a thermostatic water bath. Briefly, a homogeneous dispersed phase of 200 mL solution contained 0.25 g $FeSO_4{\cdot}7H_2O$ and 0.05 g carbon matrix (CNTs, GO, AC, CP, or BC) was obtained by ultrasonic treatment, and the Fe^{2+} ions were assumed to be adsorbed onto the negatively charged surface of carbon matrix via electrostatic attraction. Subsequently, 200 mL solution of 0.07 g $NaBH_4$ was dropwise added to generate 0.05 g nZVI that loaded on the surface of each carbon matrix (Chang et al., 2011; Schrick et al., 2004). The fresh carbon-based nZVI nanocomposites were washed three times with deoxygenated deionized water to remove impurities ions.

2.3. Batch experiments

Batch experiments were carried out in three-necked flasks with nitrogen purging and stirring (500 rpm). Unless otherwise specified, the basic conditions of CAP degradation by supported nZVI were 500 mL solution of as-prepared carbon supported nZVI nanocomposites (containing 0.1 g L^{-1} carbon and 0.1 g L^{-1} nZVI) and CAP (0.30 mM) at pH = 7.0 and T = 30 °C. Samples were collected at specified times and filtered through a 0.22 μm polyethersulfone (PES) membrane to remove the nanocomposites and quench the reaction. The PES filter does not adsorb CAP as reported in our previous study (Liu et al., 2018), and the calibration curve after PES filtration was used to calculate the CAP concentration in batch experiments which were also filtered by the same type of filter. Similar experiments were also performed in 160 mL sealed bottles (capped by Teflon Mininert valves) containing 100 mL solution and leaving 60 mL of headspace, in order to detect the accumulated H_2 in the headspace during the reaction, which was detected by GC-TCD (Agilent 6850) as previously described (Liu et al., 2005; Xu et al., 2019b). The adsorption kinetics (2 h reaction) and isotherms

(24 h reaction) of CAP by each carbon matrix were also studied via batch experiments performed in 100 mL flasks. The cytotoxicity of solution was assessed by *Escherichia Coli* (*E. coli*), and detailed assessment method of antibacterial activity is presented in the Section S1 in the Supporting Information.

2.4. Analytical methods

CAP and its degradation products were analyzed by HPLC (Agilent 1260 Infinity) and UPLC-MS/MS system (Waters Acquity™), respectively. Detailed detection methods are presented in the Section S2 and S3 in the Supporting Information. Relatively higher concentration of CAP (0.30 mM) is used in this study to meet the analytical sensitivity of HPLC, and to better compare the experimental results with previous studies regarding the removal of similar concentration of antibiotics by nZVI and other methods (Liang et al., 2013; Xia et al., 2014).

Field emission scanning electron microscopy (SEM, FEI-Quanta 200F), Brunauer-Emmett-Teller (BET, Quantachrome 02108-KR-1), Zeta potential meter (Malvern Nano-ZS90), X-ray diffraction (XRD, Rigaku-Ultima IV), energy dispersive X-ray spectroscopy (EDX, FEI-Quanta 200F), and X-ray photoelectron spectroscopy (XPS, Thermo Scientific K-Alpha) were used to characterize carbon-supported nZVI nanocomposites. Water quality analyzer (HACH HQ40d) was used to measure the oxidation reduction potential (ORP) of the carbon-supported nZVI suspension.

3. Results and discussion

3.1. Characterizations

The morphologies of bare nZVI and various carbon-supported nZVI nanocomposites were investigated by SEM and TEM with the same magnification. As shown in Figs. 1a and 2 a, serious aggregation of bare nZVI particles was observed, which was attributed to the magnetic and van der Waals forces between the nanoparticles. The nZVI particles appeared to be irregular and difficult to be distinguished after the support of AC (Fig. 1b), and several particle clusters were observed besides AC (Fig. 2b), indicating the poor distribution and reactivity of nZVI with AC support. Although spherical nZVI particles were synthesized and loaded on the surface of BC (Figs. 1c and 2 c), chain-like aggregates of nZVI were still observed. However, after the introduction of CP (Fig. 1d), no obvious aggregation or chain-like particles but more even distribution and spherical particles of nZVI were observed. Smaller nZVI particles were observed in TEM image (Fig. 2d), indicating the larger specific surface area and higher reactivity of nZVI after the support of CP, which were consistent with the results below. CNTs has been proved to be a good support for nZVI particles to inhibit their aggregation in previous studies (Xu et al., 2016b, c), and nZVI particles were loaded around the surface of CNTs (Fig. 1e), but it still seems chain-like and the distribution of nZVI was not as good as that with CP due to the self-contained chain of CNTs and their intertwined structure (Fig. 2e). As shown in Figs. 1f and 2 f, GO surface seems difficult to load nZVI particles except steric obstruction, and the distribution of nZVI particles seems better than that with CNTs support. According to the comparison of particles size and aggregation in the SEM and TEM images, it could be concluded that the distribution of nZVI particles followed an order of CP-nZVI > GO-nZVI > CNTs-nZVI > BC-nZVI > AC-nZVI > bare nZVI.

XRD was used to analyze the main components of bare nZVI, AC-nZVI, BC-nZVI, CP-nZVI, CNTs-nZVI, and GO-nZVI. As shown in Fig. 3a, the typical peak of Fe^0 at $2\theta = 45^\circ$ was observed in each spectrum, while the typical crystal surface peak of carbon 002 at $2\theta = 26^\circ$ only appeared in the spectra of CNTs-nZVI. Note that the high intensity of Fe^0 in the spectrum of AC-nZVI suggested it was much more crystalline than other carbon-supported nZVI. The typical peaks of Fe_3O_4 at $2\theta = 31^\circ/36^\circ/57^\circ$ were observed after reaction (Fig. 3b), indicated the oxidation of Fe^0 during the reaction (Liu et al., 2017). However, remaining reducibility of AC-nZVI and CP-nZVI after reaction could be expected according to the residual peak of Fe^0 in the spectra. In addition, EDX analysis was also conducted to acquire the impurities in the nanocomposites as XRD had a detection limit of 5.0 wt%. As shown in Fig. S2, the peak of O in the EDX spectra of bare nZVI indicated the inevitable oxidation of a portion of Fe^0, and the observed obvious peaks of O, P, and S in the EDX spectra of AC-nZVI suggested the impurity of AC-nZVI, while the only detected elements of Fe and C in the EDX spectra of other nanocomposites implies high-purity of prepared materials.

The chemical status of the Fe species on the surface of various

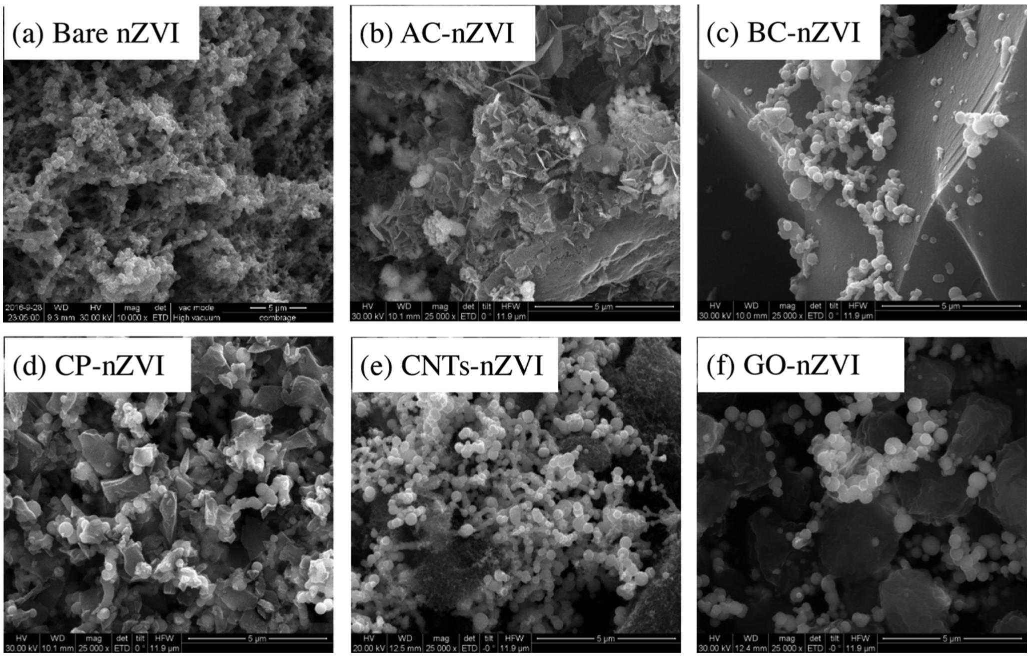

Fig. 1. SEM images of (a) bare nZVI and (b–f) carbon-based nZVI (0.1 g L^{-1} carbon matrix, 0.1 g L^{-1} nZVI).

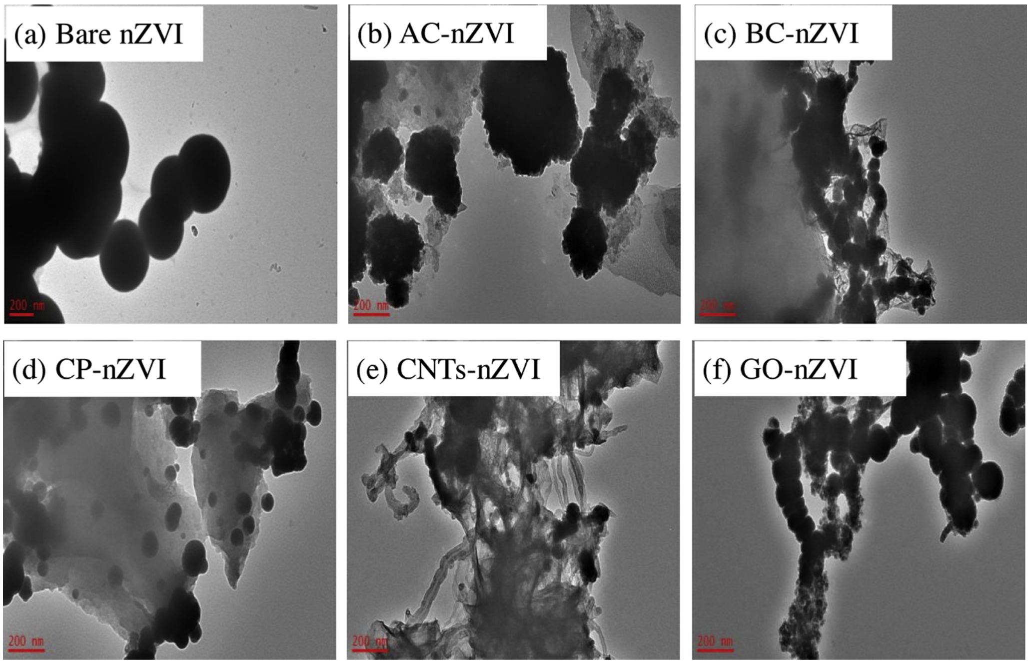

Fig. 2. TEM images of (a) bare nZVI and (b–f) carbon-based nZVI (0.1 g L^{-1} carbon matrix, 0.1 g L^{-1} nZVI).

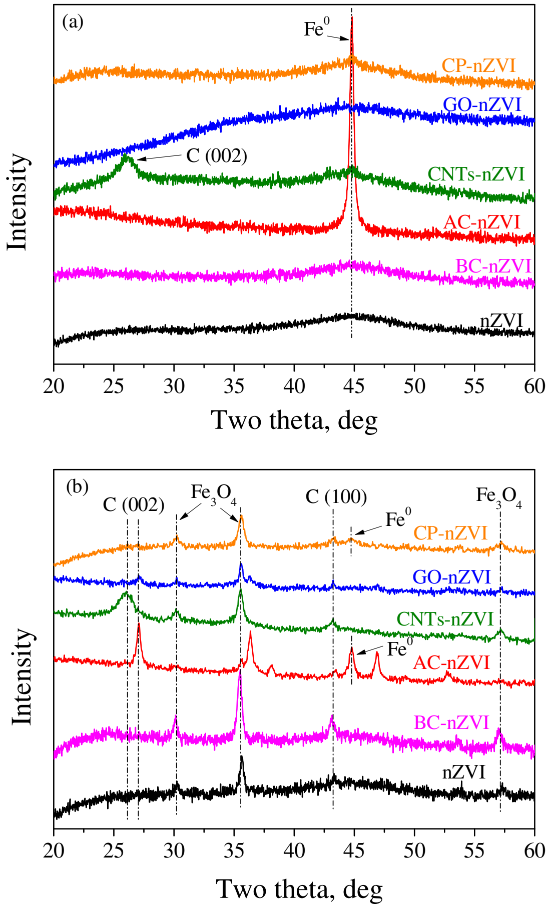

Fig. 3. XRD patterns of various carbon-based nZVI nanocomposites (a) before and (b) after reaction (T =30 °C, pH = 7.0, 0.30 mM CAP, 0.1 g L^{-1} carbon matrix, 0.1 g L^{-1} nZVI).

carbon-supported nZVI was further investigated via high resolution Fe2p XPS spectra. As shown in Fig. 4, The peaks at binding energies of ~706.7, ~719.8, ~724.8, ~711.2, ~714.6, and ~718.9/733.4 eV are characteristic of Fe^0 $2p_{1/2}$, Fe^0 $2p_{3/2}$, Fe^{3+} $2p_{1/2}$, Fe^{3+} $2p_{3/2}$, Fe^{2+} satellite, and Fe^{3+} satellite species, respectively (Xu et al., 2016c), and the detailed theoretical and experimental values of binding energies for each peak of Fe species are shown in Table S1. As reported in previous studies (Liu et al., 2018; Cao et al., 2017), iron oxides species could be observed in the nZVI samples due to the inevitably facile oxidation of nZVI surface during the preparation process. Note that the detection depth of XPS is only several nanometers, and the observation of Fe^0 peaks at ~706.8 eV suggests that the iron oxides layers of these carbon-supported nZVI before reaction were all < 10 nm (Fig. 4a–e). The peaks of Fe^0 species disappeared after reaction (Fig. 4f–j) due to the oxidation of superficial Fe^0.

3.2. Adsorption behavior of CAP by various carbon and carbon-supported nZVI

Since carbon materials have been widely reported to be good adsorbents for various contaminants (Xu et al., 2018; Yang et al., 2018; Xue et al., 2016), the adsorption behavior of CAP onto different carbon materials used in this study was also investigated. As shown in Fig. S3, the removal of CAP via the adsorption was increased with the increased dosage of AC, CP, and CNTs, while almost no CAP was removed by BC and GO. Adsorption isotherm models (Langmuir and Freundlich) and kinetics (pseudo-second-order) were used to further describe the adsorption behavior of CAP on AC, CP, and CNTs, and the fitted results of adsorption isotherms and kinetics were shown in Fig. S4 and Tables S2 and S3. AC shows much higher adsorption affinity toward CAP than other carbon materials. Since the adsorption of CAP by 0.1 g L^{-1} carbon materials (except AC) was negligible, 0.1 g L^{-1} was selected as the basic dosage of carbon materials to support nZVI particles in the CAP degradation experiments, in order to rule out the CAP adsorption by carbon materials and study the effect of different carbon supports on the reactivity of nZVI.

FTIR studies were performed to investigate the changes of surface groups before and after adsorption or reaction at the basic dosage of carbon matrices (0.1 g L^{-1}). As shown in Fig. S5a and S5b, the spectra

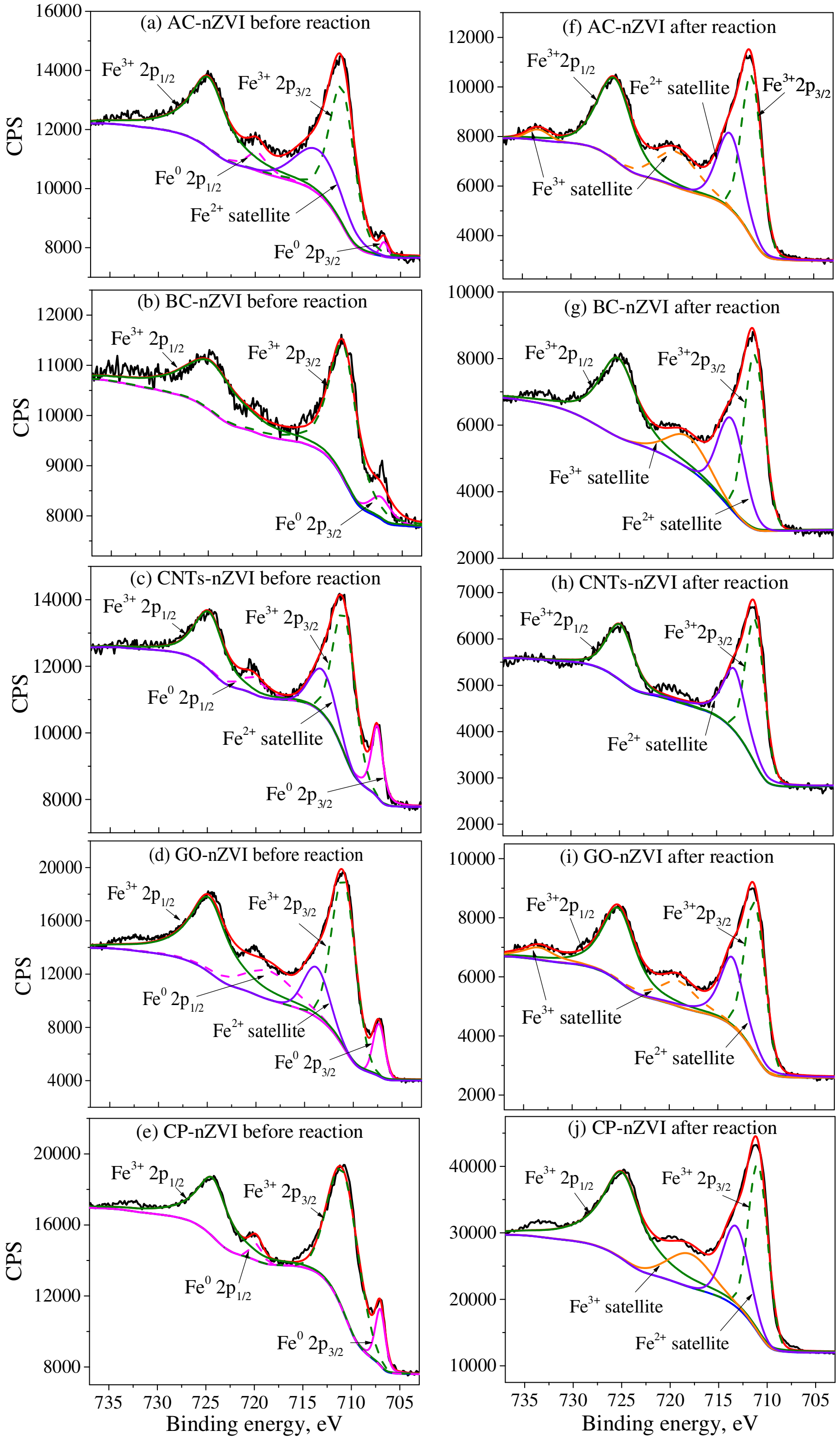

Fig. 4. Narrow scans of Fe2p XPS spectra of various carbon-based nZVI (a–e) before and (f–j) after the reaction (T = 30 °C, pH = 7.0, 0.30 mM CAP, 0.1 g L^{-1} carbon matrix, 0.1 g L^{-1} nZVI).

of AC after the adsorption of CAP were obviously changed after the adsorption of CAP, suggested that some CAP was adsorbed onto AC surface. Slight differences were observed between the spectra of other carbon materials (BC, CP, CNTs, and GO), which was probably because limited CAP (e.g. ~1% of CAP was removed by 0.1 g L^{-1} BC or GO) was adsorbed onto the surface of these carbon materials. However, there was almost no changes observed in the FTIR spectra of each carbon-supported nZVI (Fig. S5c and S5d) before and after reaction. The results of FTIR further confirmed that the adsorption of CAP onto the different carbon-based nZVI nanocomposites (except AC-nZVI) with the basic dosage of carbon matrix (0.1 g L^{-1}) could be ignored in this study, and the removal of CAP by carbon-based nZVI was mainly attributed to the reduction by nZVI, which would be easy to compare the effects of carbon types on the nZVI reactivity.

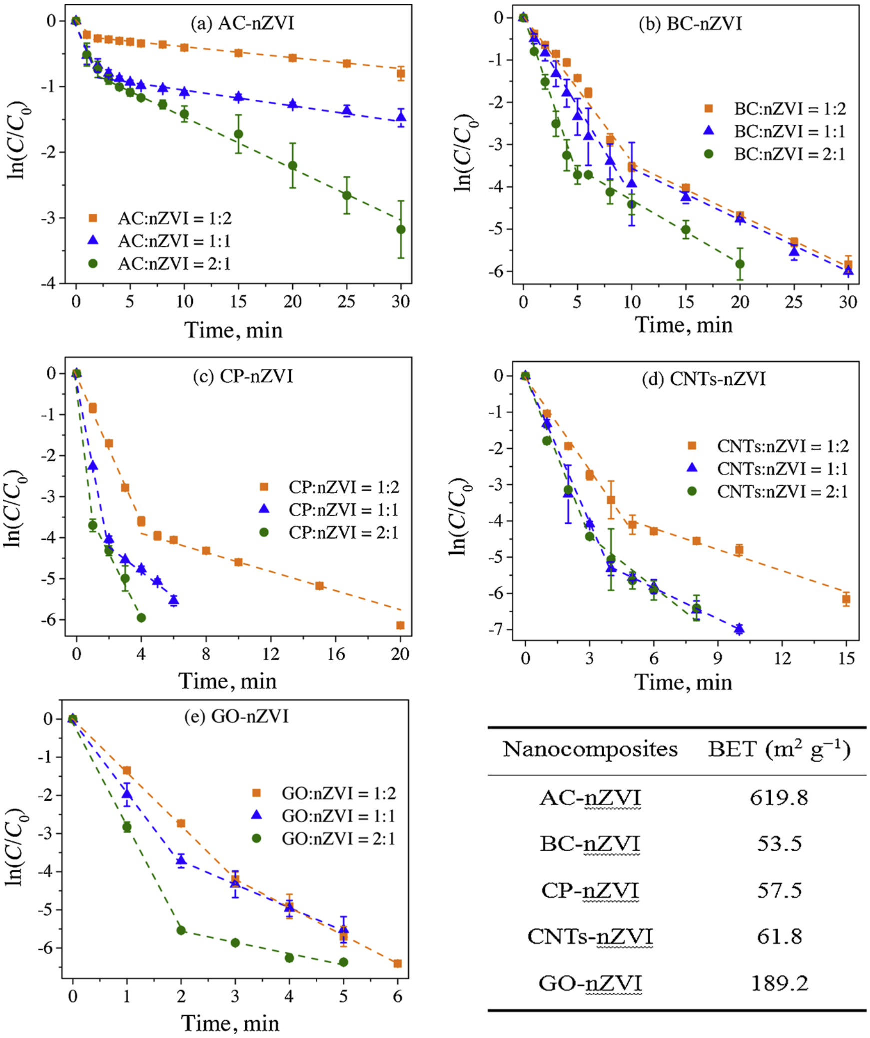

Nanocomposites	BET (m^2 g^{-1})
AC-nZVI	619.8
BC-nZVI	53.5
CP-nZVI	57.5
CNTs-nZVI	61.8
GO-nZVI	189.2

Fig. 5. Kinetics of CAP removal by (a) AC-nZVI, (b) BC-nZVI, (c) CP-nZVI, (d) CNTs-nZVI, and (e) GO-nZVI with different mass ratio of carbon/nZVI (T = 30 °C, pH = 7.0, CAP = = 0.30 mM, 0.1 g L^{-1} carbon matrix, nZVI = 0.1 g L^{-1}).

3.3. *Kinetics of CAP removal by various carbon-supported nZVI nanocomposites*

Fig. 5 shows the plots of $\ln(C_t/C_0)$ against t, and the line slope represents the removal rate according to the pseudo-first-order kinetics model. It was obvious that two slopes could be observed in most cases, indicated that the degradation process of CAP by carbon-supported nZVI nanocomposites could be divided into two stages. The possible reasons are the deactivation of surface active sites by the CAP degradation products and the surface oxidation of nZVI. The average values of R^2 of the first stage and second stage were as high as 0.994 and 0.979, respectively. The fitted values of observed removal rate (k_{obs1}) and surface-area-normalized rate (k_{SA1}) of the first stage, half life time ($t_{1/2}$), observed removal rate of the second stage (k_{obs2}), and R^2 for the removal of CAP by each carbon-supported nZVI nanocomposites are summarized in Table 1. Generally, the removal rates of CAP by nZVI were not increased after the support of AC and BC, while the CAP removals were greatly enhanced by CP-nZVI, CNTs-nZVI, and GO-nZVI nanocomposites, which could remove > 99% of CAP in 2 min. The removal kinetics followed an order of CP-nZVI > GO-nZVI > CNTs-nZVI > BC-nZVI > AC-nZVI in the first stage, which was consistent with the distribution results that observed in the SEM and TEM images (Figs. 1 and 2). Although AC showed highest adsorption capacity toward CAP even at the basic dosage (0.1 g L^{-1}) according to the previous results (Figs. S3 and S4), the removal rate of CAP by AC-nZVI was

Table 1
Kinetics parameters for the removal of aqueous CAP by various carbon-based nZVI with different mass ratio of carbon/nZVI (T = 30 °C, pH = 7.0, CAP = 0.30 mM, nZVI = 0.1 g L^{-1}).

Materials	C:Fe	k_{obs1}	$t_{1/2}$	k_{SA1}	R^2	k_{obs2}	R^2
Bare nZVI	–	0.74	0.94	1.13	0.997	0.19	0.997
AC-nZVI	1:2	0.21	3.30	–	1.000	0.02	0.981
	1:1	0.52	1.33	0.004	1.000	0.03	0.915
	2:1	0.51	1.36	–	1.000	0.08	0.979
BC-nZVI	1:2	0.33	2.10	–	0.973	0.12	0.994
	1:1	0.43	1.61	0.04	0.984	0.12	0.995
	2:1	0.78	0.89	–	0.992	0.15	0.994
CP-nZVI	1:2	0.90	0.77	–	0.998	0.12	0.997
	1:1	2.07	0.33	0.18	0.994	0.30	0.942
	2:1	3.70	0.19	–	1.000	0.78	0.995
CNTs-nZVI	1:2	0.86	0.81	–	0.988	0.20	0.940
	1:1	1.38	0.50	0.11	0.984	0.29	0.999
	2:1	1.53	0.45	–	0.991	0.47	0.959
GO-nZVI	1:2	1.39	0.50	–	0.999	0.74	0.999
	1:1	1.86	0.37	0.05	0.999	0.61	0.999
	2:1	2.77	0.25	–	0.999	0.30	0.974

k_{obs1} (min^{-1}) and k_{obs2} (min^{-1}) are the observed pseudo-first-order rate constant of CAP removal in the first fast and second slow stages, respectively; $t_{1/2}$ stands for the half-life calculated from the first-order decay fitting using k_{obs1}; k_{SA1} (L min^{-1} m^{-2}) represents the surface-area-normalized reaction rate of CAP removal in the first fast stage.

much lower than that by bare nZVI, indicating the poor distribution of nZVI by AC and the reduction of CAP by nZVI was the dominant pathway for CAP removal in this study. Since the adsorption of CAP by BC and GO were negligible under the dosages used for nZVI stabilization (Fig. S3), the higher removal rate of CAP at higher C/Fe mass ratio was probably attributed to the better distribution of nZVI particles with more efficient support. The values of k_{obs1} (2.07 min^{-1}), k_{SA1} (0.18 L min^{-1} m^{-2}), and k_{obs2} (0.30 min^{-1}) of CAP removal by CP-nZVI were much higher than those of other carbon-based nZVI nanocomposites, and it only required 0.33 min to remove half of the CAP. No H_2 was detected after 30 min reaction, indicating that the reduction of CAP by nZVI was much faster than the reduction of water by nZVI ($Fe^0 + 2H_2O \rightarrow Fe^{2+} + 2OH^- + H_2$). The H_2 limit of quantitation (LOQ) of our GC-TCD is ~1 μmol, the reduction of CAP requires at least 2 e^- per molar (reduced to the primary intermediate, CAP − O). Once all the 0.03 mmol CAP was removed, it required at least 0.06 mmol, while the H_2 was below the LOQ (1 μmol) and electrons for H_2 evolution were less than 2 μmol, hence, the electron efficiency for CAP was > 0.06 mmol/(0.06 mmol + 2 μmol), that is > 97%. Almost all the electrons from Fe^0 were utilized for the degradation of CAP. In addition, the removal rate of CAP by CP-nZVI in this study was ~10 and 240 times higher than that by nZVI stored in ethanol and a biocathode method, respectively (Liang et al., 2013; Xia et al., 2014). These results also suggested the application of nZVI would be promising when a contaminant could be quickly removed and outcompete with water for the electrons from nZVI.

3.4. Proposed mechanism of CAP removal by carbon-supported nZVI nanocomposites

UPLC-MS/MS analysis was performed to detect the potential products of CAP by carbon-supported nZVI nanocomposites, in order to elucidate the entire pathway of CAP removal. Detailed mass spectrums from the UPLC-MS/MS analysis are shown in Figs. S5–S8, which clearly describe the changes of reduction products of CAP ($C_{11}H_{12}Cl_2N_2O_5$) by carbon-based nZVI nanocomposites during the reaction. Note that no residual CAP was detected by UPLC-MS/MS after the reaction, indicating that nZVI and carbon-supported nZVI were also efficient for the removal of trace CAP that below the LOQ of UPLC-MS/MS (~0.2 ng L^{-1}). Fig. 6a summarizes the reduction products based on the results of UPLC-MS/MS analysis, as well as the proposed pathway of CAP removal by carbon-supported nZVI nanocomposites. First, the cleavage of coordination bond between O atom and N atom in the NO_2 group occurred, generating the first intermediate product with a MW of 307 ($C_{11}H_{12}Cl_2N_2O_4$). This product was quickly generated and then degraded by reactive CP-nZVI, CNTs-nZVI, and GO-nZVI nanocomposites (Fig. S6), which was the main reason for the rapid removal of CAP by these nanocomposites. As the reaction proceeded, the other O atom on the NO_2 group was removed, and the NO_2 group was completely converted to NH_2 group at this time, which was inferred by the detection of production-293 ($C_{11}H_{14}ClN_2O_3$) (Fig. S7). Then, the detection of production-259 ($C_{11}H_{15}ClN_2O_3$) (Fig. S8) indicated the removal of one Cl atom from product-293 via dechlorination. Finally, product-224 ($C_{11}H_{16}N_2O_3$) (Fig. S9) was detected after the removal of the second Cl atom via dechlorination. Both denitration and dechlorination of CAP by carbon supported nZVI were confirmed by the products analysis by UPCL-MS/MS.

Note that no obvious difference was observed between the XRD spectra (except AC-nZVI) and XPS spectra of different carbon-supported nZVI nanocomposites (Figs. 3 and 4), and the adsorption of CAP on different carbon-supported nZVI nanocomposites were negligible under the basic dosage of carbon matrix (0.1 g L^{-1}) as shown in Fig. S3. It requires 2 and 10 mol e^- to reduce each mole CAP to the preliminary product ($C_{11}H_{12}Cl_2N_2O_4$) and the final product ($C_{11}H_{16}N_2O_3$), respectively, and each mole Fe^0 could provide 2 and 3 mol e^- when it was oxidized to Fe^{2+} and Fe^{3+}, respectively. Electrons from 0.1 g L^{-1} (1.8 mM) nZVI with ~95% Fe^0 content were sufficient for the removal of 0.30 mM CAP. Hence, the removal of CAP by these carbon-based nZVI nanocomposites was mainly controlled by the distribution of nZVI, which deeply affects the reactivity of nZVI for CAP removal in this study. Fig. 6b shows the schematic of distribution and reactivity of various carbon-based nZVI nanocomposites based on the SEM/TEM images (Figs. 1 and 2) and CAP removal kinetics (Fig. 5).

3.5. Performance of carbon-supported nZVI nanocomposites for CAP removal under different pH

The isoelectric point of AC-nZVI, BC-nZVI, CP-nZVI, CNTs-nZVI, and GO-nZVI was around 6.3, 9.0, 7.9, 5.8, and 5.0, respectively (Fig. S10). The removal efficiency of CAP after 1 min reaction was decreased when the initial solution pH increased (Fig. 7a). The pK_a value of CAP is 7.59, and no electrical repulsion would occur when pH < pKa because CAP is in non-ionized form. Both CAP molecules and carbon-based nZVI nanocomposites were negatively charged when pH increased from 7.0 to 9.0, which might reduce the reaction rate due to the electrostatic repulsion. Besides the electrostatic interactions, the corrosion of nZVI was another important factor. Generally, nZVI would be deactivated by the formation of (hydro)oxides on the surface under alkaline condition. However, after 30 min reaction (Fig. 7b), all the CAP was removed by CP-nZVI, CNTs-nZVI, and GO-nZVI in the pH range of 3.0–9.0, suggesting the high pH-tolerance and reactivity of these carbon-supported nZVI nanocomposites for the removal of CAP.

3.6. Assessment of antibacterial activity of CAP-contaminated solution after reaction

Since nZVI or carbon-supported nZVI treatment under anaerobic condition did not completely degrade CAP, and the toxicity of CAP degradation products was further studied to determine whether another process needed to be followed. *E. coli.* was used to evaluate the antibacterial activity of CAP-contaminated solution before and after reaction. Fig. 8 shows the numbers of *E. coli* and the MS signal values of different products. Approximately 49 and 47 (numbers) *E. coli* grew in the blank medium and the medium with filtrate of bare nZVI suspension, respectively, suggesting that the effect of iron ions on the toxicity was negligible, and the toxicity of nZVI particles would be also limited when using them in the permeable reactive barriers (PRB) that maintain nZVI particles in the barriers and only iron ions would be released to the environment. No *E. coli* grew in the control experiment with 0.009 mM CAP (the minimal inhibitory concentration), while 16, 68, 71, 81, and 59 (numbers) *E. coli* grew with the addition of solution that treated by AC-nZVI, BC-nZVI, CP-nZVI, CNTs-nZVI, and GO-nZVI, respectively. The antibacterial activities of CAP contaminated solutions were all obviously decreased after the treatments by these carbon-supported nZVI nanocomposites. And based on MS signal values of degraded products (Fig. 8), it also could be concluded that the antibacterial activity would be decreased with the proceeding of CAP degradation, suggesting that partial degradation (denitration and dechlorination) was enough to take away the antimicrobial properties. Moreover, more *E. coli* was observed in the presence of degraded products of CAP, indicating the degraded products were likely to be nutrient source for the growth of *E. coli.* These results revealed that carbon-supported nZVI was a promising alternative to remediate CAP-contaminated water to reduce the antibiotic selection pressure of the environment.

3.7. Capacity and electron utilization of CP-nZVI nanocomposite for CAP removal

Since CP-nZVI nanocomposite shows good nZVI distribution, high reactivity, low antibacterial activity, and high pH-tolerance (Fig. 7), the capacity and reusability of CP-nZVI nanocomposite was further

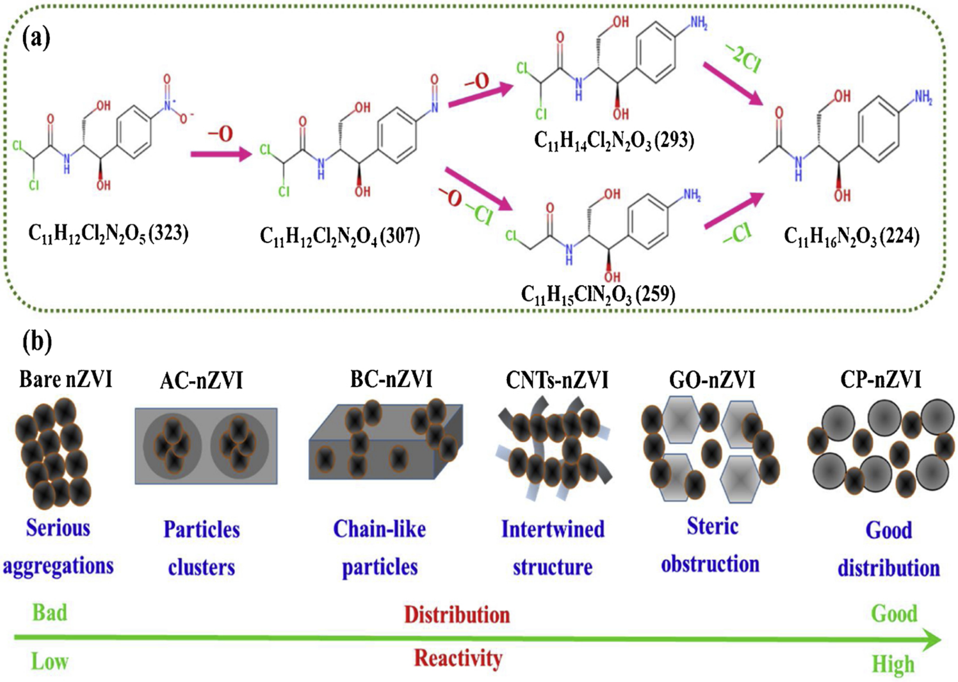

Fig. 6. Mechanism of CAP removal by carbon-based nZVI nanocomposites, (a) proposed pathway and (b) schematic of distribution and reactivity of various carbon-based nZVI nanocomposites.

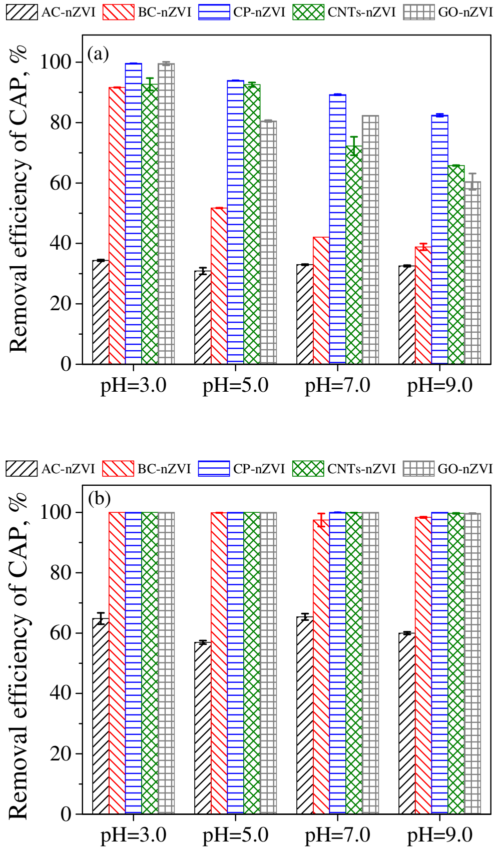

Fig. 7. Performance of carbon-based nZVI nanocomposites for CAP removal under different pH, (a) after 1 min reaction and (b) after 30 min reaction (T = 30 °C, carbon matrix = 0.1 g L^{-1}, nZVI = 0.1 g L^{-1}).

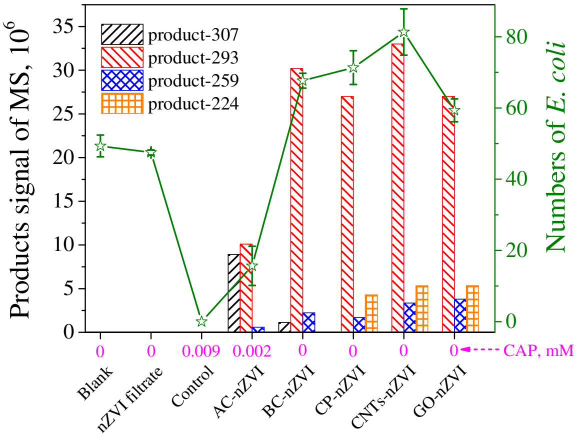

Fig. 8. Assessment of the antibacterial activity of reaction solution after 30 min reaction (T = 30 °C, pH = 7.0, CAP = 0.30 mM, carbon matrix = 0.1 g L^{-1}, nZVI = 0.1 g L^{-1}; Blank: pure medium without contaminant; nZVI filtrate: medium with filtrate of 0.1 g L^{-1} bare nZVI suspension without contaminant; Control: medium with 0.009 mM CAP).

investigated by adding consecutive doses of 0.30 mM CAP and allowing 60 min reaction time between doses. Oxidation-reduction potential (ORP) is a measure of electron activity in a solution and indicates its relative tendency to accept or transfer electrons (Elliott and Zhang, 2001; Yu et al., 2014), and the ORP was also measured during the consecutive reaction. As shown in Fig. 9, the ORP was sharply increased upon adding CAP solution with high ORP (32 mV). The ORP value trended to drop during the first two runs and all the CAP was removed, suggested the generation of electrons and the proceeding of nZVI corrosion. Although almost all the CAP was removed within 5 min in Run 3, the solution ORP did not come back after CAP addition and quickly increased to approximately −200 mV at the end of Run 3, indicating the depletion of Fe^0. Moreover, no CAP was removed in Runs 4 and 5 when the solution ORP was higher than −200 mV, which proposed a convenient method to check the reactivity of nZVI for CAP removal.

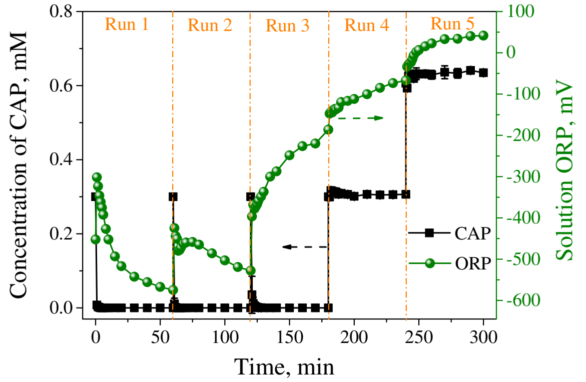

Fig. 9. Reusability of CP-nZVI for CAP removal (T = 30 °C, pH = 7.0, CP = 0.1 g L^{-1}, nZVI = 0.1 g L^{-1}, 0.30 mM CAP added at the beginning of each run).

The accumulated H_2 after 5 runs was accounted for ~8% electron-equivalents of the initial nZVI, suggesting that more than 90% of the electrons were utilized for the degradation of CAP. At least 0.90 mM CAP (3 runs) could be removed by 1.8 mM nZVI (0.1 g L^{-1}) supported by CP via experiments of 60 min each run, suggesting the capacity of nZVI for CAP removal could achieved to 3000 mg g^{-1}. Note that 60 min for each run was excessive for CAP removal and a portion of electrons were used to react with water after CAP was removed, hence, higher CAP capacity (> 3000 mg g^{-1}) and electron efficiency (> 90%) are expected after optimizing the time of each run.

3.8. Application potential of carbon supported nZVI nanocomposite for CAP removal

The removal rates of CAP by nZVI in different water matrices were found to be not decreased compared to ultrapure water in our previous study (Liu et al., 2018), indicating that the other substances and metals did not affect the degradation of CAP by nZVI. Since the reactivity (k_{obs}) of CP-nZVI with CAP was 5 times higher than that of nZVI (Table 1), it could be anticipated that the CP-nZVI nanocomposites will be a more robust material for CAP removal in different water matrices. Note that the dose of nZVI was only 0.1 g L^{-1}, but its capacity for CAP was up to 3000 mg g^{-1} with fast rate and almost complete utilization of electrons. Moreover, the resulted nZVI sludge could be even much smaller if the CAP concentration is lower than that studied in this work, and the toxicity of nZVI particles would be also limited, especially using them in the PRB, which maintains nZVI particles in the barriers and only allows iron ions to be released to the environment, and the iron filtrate had been proved to be have almost no toxic effect on the *E.coli.* growth (Fig. 8). This study also suggests that partial degradation of CAP (denitration and dechlorination) was enough to take away the antimicrobial properties, and the products could probably be utilized as nutrients to favor the growth of *E. coli.* (Fig. 8). These results suggest the high application potential of nZVI for CAP-contaminated water.

It is difficult to estimate the total potential cost of nZVI for future application at larger scale, many factors (e.g. order amount, transportation cost, hydrogeological and geochemical investigations, conducting a pilot test, etc.) will affect the overall costs (Stefaniuk et al., 2016). Generally, nZVI is considered as a cost-effective and efficient technology for *in-situ* remediation. Although the initial investment may be higher than other methods, all the cost of the remediation with nZVI in the permeable reactive barrier arise within one or two years, while the costs of pump and treat of other methods are spread over other 10–20 years (Mueller et al., 2012). However, for the carbon supported nZVI, the carbon is just added into the Fe ion solution before its reduction by $NaBH_4$, almost no extra energy is required for the formation of carbon supported nZVI compared with nZVI. Moreover, carbon supports have been reported to be good carriers for enhancing the transportation of nZVI in field-scale remediation (Schrick et al., 2004; Busch et al., 2015, 2014; Su et al., 2016).

4. Conclusions

Fast degradation, high capacity, and high electron efficiency of CAP removal was achieved by carbon-supported nZVI in this study. The chemical compositions of AC-nZVI, BC-nZVI, CP-nZVI, CNTs-nZVI, and GO-nZVI were similar, while the distributions of nZVI particles were different with different carbon support, and nZVI particles were most dispersive with CP support. For the 0.30 mM CAP removal by carbon-supported nZVI with a C:Fe ratio of 2:1 (nZVI dose was 0.1 g L^{-1}), the removal kinetics rate constant (k_{obs}) followed an order of CP-nZVI (3.70 min^{-1}) > GO-nZVI (2.77 min^{-1}) > CNTs-nZVI (1.53 min^{-1}) > BC-nZVI (0.78 min^{-1}) > AC-nZVI (0.51 min^{-1}), and the half-life of CAP was only 0.19 min, 0.25 min, 0.45 min, 0.89 min, and 1.36 min respectively. These trends were consistent with the distribution results that observed in the SEM and TEM images. Consecutive experiments suggest that the capacity of CP-supported nZVI for CAP was at least 3000 mg g^{-1}. Based on the UPLC-MS/MS analysis, the mechanisms of denitration and dechlorination of CAP by various carbon-supported nZVI nanocomposites were summarized, and the distribution of nZVI particles was considered as the main factor of nZVI reactivity in this study. The antibacterial activity of CAP-contaminated solution would be greatly decreased with the proceeding of CAP degradation. CAP could outcompete with water for the electrons from nZVI, and almost all the electrons of nZVI would be utilized to degrade CAP in consecutive experiments. These results suggested that carbon-supported nZVI was a promising alternative to remediate CAP-contaminated water to reduce the antibiotic selection pressure of the environment.

Acknowledgements

The authors would like to acknowledge the Chenguang Program of Shanghai Education Development Foundation and Shanghai Municipal Education Commission (No.16CG23) and the National Natural Science Foundation of China (No.41771506) for their financial support.

Appendix A. Supplementary data

Supplementary material related to this article can be found, in the online version, at doi:https://doi.org/10.1016/j.jhazmat.2019.121253.

References

Ahmed, M.B., Zhou, J.L., Ngo, H.H., Guo, W., Thomaidis, N.S., Xu, J., 2017. Progress in the biological and chemical treatment technologies for emerging contaminant removal from wastewater: a critical review. J. Hazard. Mater. 323, 274–298.

Arancibia-Miranda, N., Baltazar, S.E., García, A., Muñoz-Lira, D., Sepúlveda, P., Rubio, M.A., Altbir, D., 2016. Nanoscale zero valent supported by Zeolite and Montmorillonite: template effect of the removal of lead ion from an aqueous solution. J. Hazard. Mater. 301, 371–380.

Boparai, H.K., Joseph, M., Carroll, D.M.O., 2011. Kinetics and thermodynamics of cadmium ion removal by adsorption onto nano zerovalent iron particles. J. Hazard. Mater. 186, 458–465.

Busch, J., Meißner, T., Potthoff, A., Bleyl, S., Georgi, A., Mackenzie, K., Trabitzsch, R., Werban, U., Oswald, S.E., 2015. A field investigation on transport of carbon-supported nanoscale zero-valent iron (nZVI) in groundwater. J. Contam. Hydrol. 181, 59–68.

Busch, J., Meißner, T., Potthoff, A., Oswald, S.E., 2014. Transport of carbon colloid supported nanoscale zero-valent iron in saturated porous media. J. Contam. Hydrol. 164, 25–34.

Cao, Z., Liu, X., Xu, J., Zhang, J., Yang, Y., Zhou, J., Xu, X., Lowry, G.V., 2017. Removal of antibiotic florfenicol by sulfide-modified nanoscale zero-valent iron. Environ. Sci. Technol. 51, 11269–11277.

Chang, C., Lian, F., Zhu, L., 2011. Simultaneous adsorption and degradation of γ-HCH by nZVI/Cu bimetallic nanoparticles with activated carbon support. Environ. Pollut. 159, 2507–2514.

Chen, Y., Zhou, J.L., Cheng, L., Zheng, Y.Y., Xu, J., 2017. Sediment and salinity effects on the bioaccumulation of sulfamethoxazole in zebrafish (Danio rerio). Chemosphere 180, 467–475.

Elliott, D.W., Zhang, W., 2001. Field assessment of nanoscale bimetallic particles for groundwater treatment. Environ. Sci. Technol. 35, 4922–4926.

Guo, X., Yang, Y., Lu, D., Niu, Z., Feng, J., Chen, Y., Tou, F., Garner, E., Xu, J., Liu, M., Hochella, M.F., 2018. Biofilms as a sink for antibiotic resistance genes (ARGs) in the Yangtze Estuary. Water Res. 129, 277–286.

He, F., Li, Z., Shi, S., Xu, W., Sheng, H., Gu, Y., Jiang, Y., Xi, B., 2018. Dechlorination of excess trichloroethene by bimetallic and sulfidated nanoscale zero-valent iron. Environ. Sci. Technol. 52, 8627–8637.

Hoch, L.B., Mack, E.J., Hydutsky, B.W., Hershman, J.M., Skluzacek, J.M., Mallouk, T.E., 2008. Carbothermal synthesis of carbon-supported nanoscale zero-valent iron particles for the remediation of hexavalent chromium. Environ. Sci. Technol. 42, 2600–2605.

Hu, X., Zhou, Q., Luo, Y., 2010. Occurrence and source analysis of typical veterinary antibiotics in manure, soil, vegetables and groundwater from organic vegetable bases, northern China. Environ. Pollut. 158, 2992–2998.

Hwang, Y., Lee, Y., Mines, P.D., Huh, Y.S., Andersen, H.R., 2014. Nanoscale zero-valent iron (nZVI) synthesis in a Mg-aminoclay solution exhibits increased stability and reactivity for reductive decontamination. Appl. Catal. B Environ. 147, 748–755.

Joo, S.H., Feitz, A.J., Waite, T.D., 2004. Oxidative degradation of the carbothioate herbicide, molinate, using nanoscale zero-valent iron. Environ. Sci. Technol. 38, 2242–2247.

Li, Y., Cheng, W., Sheng, G., Li, J., Dong, H., Chen, Y., Zhu, L., 2015. Synergetic effect of a pillared bentonite support on SE(VI) removal by nanoscale zero valent iron. Appl. Catal. B Environ. 174, 329–335.

Li, J., Zhang, X., Liu, M., Pan, B., Zhang, W., Shi, Z., Guan, X., 2018. Enhanced reactivity and electron selectivity of sulfidated zerovalent iron toward chromate under aerobic conditions. Environ. Sci. Technol. 52, 2988–2997.

Liang, B., Cheng, H., Kong, D., Gao, S., Sun, F., Cui, D., Kong, F., Zhou, A., Liu, W., Ren, N., Wu, W., Wang, A., Lee, D., 2013. Accelerated reduction of chlorinated nitroaromatic antibiotic chloramphenicol by biocathode. Environ. Sci. Technol. 47, 5353–5361.

Liu, Yueqiang, Sara, A.M., Robert, D.T., And, D.S.S., Gregory, V.L., 2005. TCE dechlorination rates, pathways, and efficiency of nanoscale iron particles with different properties. Environ. Sci. Technol. 39, 1338–1345.

Liu, A., Liu, J., Han, J., Zhang, W., 2017. Evolution of nanoscale zero-valent iron (nZVI) in water: microscopic and spectroscopic evidence on the formation of nano- and microstructured iron oxides. J. Hazard. Mater. 322, 129–135.

Liu, X., Cao, Z., Yuan, Z., Zhang, J., Guo, X., Yang, Y., He, F., Zhao, Y., Xu, J., 2018. Insight into the kinetics and mechanism of removal of aqueous chlorinated nitroaromatic antibiotic chloramphenicol by nanoscale zero-valent iron. Chem. Eng. J. 334, 508–518.

Lv, D., Zhou, J., Cao, Z., Xu, J., Liu, Y., Li, Y., Yang, K., Lou, Z., Lou, L., Xu, X., 2019. Mechanism and influence factors of chromium(VI) removal by sulfide-modified nanoscale zerovalent iron. Chemosphere 224, 306–315.

Mueller, N.C., Braun, J., Bruns, J., Černík, M., Rissing, P., Rickerby, D., Nowack, B., 2012. Application of nanoscale zero valent iron (NZVI) for groundwater remediation in Europe. Environ. Sci. Pollut. Res. 19, 550–558.

Nurmi, J.T., Tratnyek, P.G., Sarathy, V., Baer, D.R., Amonette, J.E., Pecher, K., Wang, C., Linehan, J.C., Matson, D.W., Penn, R.L., Driessen, M.D., 2005. Characterization and properties of metallic iron nanoparticles: spectroscopy, electrochemistry, and kinetics. Environ. Sci. Technol. 39, 1221–1230.

Phenrat, T., Saleh, N., Sirk, K., Tilton, R.D., Lowry, G.V., 2007. Aggregation and sedimentation of aqueous nanoscale zerovalent iron dispersions. Environ. Sci. Technol. 41, 284–290.

Qiao, J., Song, Y., Sun, Y., Guan, X., 2018. Effect of solution chemistry on the reactivity and electron selectivity of zerovalent iron toward Se(VI) removal. Chem. Eng. J. 353, 246–253.

Qin, H., Li, J., Yang, H., Pan, B., Zhang, W., Guan, X., 2017. Coupled effect of ferrous ion and oxygen on the electron selectivity of zerovalent iron for selenate sequestration. Environ. Sci. Technol. 51, 5090–5097.

Schrick, B., Hydutsky, B.W., Blough, J.L., Mallouk, T.E., 2004. Delivery vehicles for zerovalent metal nanoparticles in soil and groundwater. Chem. Mater. 16, 2187–2193.

Sheng, G., Hu, J., Li, H., Li, J., Huang, Y., 2016. Enhanced sequestration of Cr(VI) by nanoscale zero-valent iron supported on layered double hydroxide by batch and XAFS study. Chemosphere 148, 227–232.

Stefaniuk, M., Oleszczuk, P., Ok, Y.S., 2016. Review on nano zerovalent iron (nZVI): from synthesis to environmental applications. Chem. Eng. J. 287, 618–632.

Su, H., Fang, Z., Tsang, P.E., Fang, J., Zhao, D., 2016. Stabilisation of nanoscale zerovalent iron with biochar for enhanced transport and in-situ remediation of hexavalent chromium in soil. Environ. Pollut. 214, 94–100.

Tang, J., Tang, L., Feng, H., Zeng, G., Dong, H., Zhang, C., Huang, B., Deng, Y., Wang, J., Zhou, Y., 2016. PH-dependent degradation of p-nitrophenol by sulfidated nanoscale zerovalent iron under aerobic or anoxic conditions. J. Hazard. Mater. 320, 581–590.

Tang, L., Tang, J., Zeng, G., Yang, G., Xie, X., Zhou, Y., Pang, Y., Fang, Y., Wang, J., Xiong, W., 2015. Rapid reductive degradation of aqueous p-nitrophenol using nanoscale zero-valent iron particles immobilized on mesoporous silica with enhanced antioxidation effect. Appl. Surf. Sci. 333, 220–228.

Titirici, M., White, R.J., Brun, N., Budarin, V.L., Su, D.S., Del Monte, F., Clark, J.H., MacLachlan, M.J., 2015. Sustainable carbon materials. Chem. Soc. Rev. 44, 250–290.

Wang, C., Zhang, W., 1997. Synthesizing nanoscale iron particles for rapid and complete dechlorination of TCE and PCBs. Environ. Sci. Technol. 31, 2154–2156.

Wu, X., Yang, Q., Xu, D., Zhong, Y., Luo, K., Li, X., Chen, H., Zeng, G., 2013. Simultaneous adsorption/reduction of bromate by nanoscale zerovalent iron supported on modified activated carbon. Ind. Eng. Chem. Res. 52, 12574–12581.

Xia, S., Gu, Z., Zhang, Z., Zhang, J., Hermanowicz, S.W., 2014. Removal of chloramphenicol from aqueous solution by nanoscale zero-valent iron particles. Chem. Eng. J. 257, 98–104.

Xu, J., Cao, Z., Zhang, Y., Yuan, Z., Lou, Z., Xu, X., Wang, X., 2018. A review of functionalized carbon nanotubes and graphene for heavy metal adsorption from water: preparation, application, and mechanism. Chemosphere 195, 351–364.

Xu, J., Cao, Z., Wang, Y., Zhang, Y., Gao, X., Ahmed, M.B., Zhang, J., Yang, Y., Zhou, J.L., Lowry, G.V., 2019a. Distributing sulfidized nanoscale zerovalent iron onto phosphorus-functionalized biochar for enhanced removal of antibiotic florfenicol. Chem. Eng. J. 359, 713–722.

Xu, J., Lv, X., Li, J., Li, Y., Shen, L., Zhou, H., Xu, X., 2012a. Simultaneous adsorption and dechlorination of 2,4-dichlorophenol by Pd/Fe nanoparticles with multi-walled carbon nanotube support. J. Hazard. Mater. 225–226, 36–45.

Xu, J., Tang, J., Baig, S.A., Lv, X., Xu, X., 2013a. Enhanced dechlorination of 2,4-dichlorophenol by Pd/Fe-Fe_3O_4 nanocomposites. J. Hazard. Mater. 244–245, 628–636.

Xu, J., Cao, Z., Liu, X., Zhao, H., Xiao, X., Wu, J., Xu, X., Zhou, J.L., 2016a. Preparation of functionalized Pd/Fe-Fe_3O_4@MWCNTs nanomaterials for aqueous 2,4-dichlorophenol removal: Interactions, influence factors, and kinetics. J. Hazard. Mater. 317, 656–666.

Xu, J., Tan, L., Baig, S.A., Wu, D., Lv, X., Xu, X., 2013b. Dechlorination of 2,4-dichlorophenol by nanoscale magnetic Pd/Fe particles: effects of pH, temperature, common dissolved ions and humic acid. Chem. Eng. J. 231, 26–35.

Xu, J., Hao, Z., Xie, C., Lv, X., Yang, Y., Xu, X., 2012b. Promotion effect of Fe^e and Fe_3O_4 on nitrate reduction using zero-valent iron. Desalination 284, 9–13.

Xu, J., Wang, Y., Weng, C., Bai, W., Jiao, Y., Kaegi, R., Lowry, G.V., 2019b. Reactivity, selectivity, and long-term performance of sulfidized nanoscale zerovalent iron with different properties. Environ. Sci. Technol. 53, 5936–5945.

Xu, J., Liu, X., Lowry, G.V., Cao, Z., Zhao, H., Zhou, J.L., Xu, X., 2016b. Dechlorination mechanism of 2,4-dichlorophenol by magnetic MWCNTs supported Pd/Fe nanohybrids: rapid adsorption, gradual dechlorination, and desorption of phenol. ACS Appl. Mater. Inter. 8, 7333–7342.

Xu, J., Sheng, T., Hu, Y., Baig, S.A., Lv, X., Xu, X., 2013c. Adsorption–dechlorination of 2,4-dichlorophenol using two specified MWCNTs-stabilized Pd/Fe nanocomposites. Chem. Eng. J. 219, 162–173.

Xu, J., Lv, X., Li, J., Li, Y., Shen, L., Zhou, H., Xu, X., 2012c. Simultaneous adsorption and dechlorination of 2,4-dichlorophenol by Pd/Fe nanoparticles with multi-walled carbon nanotube support. J. Hazard. Mater. 225–226, 36–45.

Xu, H., Sun, Y., Li, J., Li, F., Guan, X., 2016c. Aging of zerovalent iron in synthetic groundwater: X-ray photoelectron spectroscopy depth profiling characterization and depassivation with uniform magnetic field. Environ. Sci. Technol. 50, 8214–8222.

Xue, X., Xu, J., Baig, S.A., Xu, X., 2016. Synthesis of graphene oxide nanosheets for the removal of Cd(II) ions from acidic aqueous solutions. J. Taiwan Inst. Chem. E. 59, 365–372.

Yang, K., Lou, Z., Fu, R., Zhou, J., Xu, J., Baig, S.A., Xu, X., 2018. Multiwalled carbon nanotubes incorporated with or without amino groups for aqueous Pb(II) removal: comparison and mechanism study. J. Mol. Liq. 260, 149–158.

Yu, R., Chi, F., Cheng, W., Chang, J., 2014. Application of pH, ORP, and DO monitoring to evaluate chromium(VI) removal from wastewater by the nanoscale zero-valent iron (nZVI) process. Chem. Eng. J. 255, 568–576.

Zhao, H., Cao, Z., Liu, X., Zhan, Y., Zhang, J., Xiao, X., Yang, Y., Zhou, J., Xu, J., 2017. Seasonal variation, flux estimation, and source analysis of dissolved emerging organic contaminants in the Yangtze Estuary, China. Mar. Pollut. Bull. 125, 208–215.

Zou, Y., Wang, X., Khan, A., Wang, P., Liu, Y., Alsaedi, A., Hayat, T., Wang, X., 2016. Environmental remediation and application of nanoscale zero-valent iron and its composites for the removal of heavy metal ions: a review. Environ. Sci. Technol. 50, 7290–7304.